Estimation of Surface Sensible Heat Flux due to Precipitation over CONUS and Its Impact on Urban Extreme Precipitation Modeling

HAOCHEN TAN,[a] RAO KOTAMARTHI,[a] AND PALLAV RAY[b]

[a] *Environmental Science Division (EVS), Argonne National Laboratory, Lemont, Illinois*
[b] *Meteorology, Florida Institute of Technology, Melbourne, Florida*

(Manuscript received 3 May 2023, in final form 10 January 2024, accepted 17 January 2024)

ABSTRACT: The surface sensible heat flux induced by precipitation (Q_P) is a consequence of the temperature difference between the surface and the rain droplets. Despite its seemingly negligible nature, Q_P is frequently omitted from both meteorological and climatological models. Nevertheless, it is important to acknowledge the numerous occasions in which the instantaneous values of Q_P can be significant, particularly during extreme precipitation events. This study undertakes a comprehensive assessment of Q_P across the contiguous United States (CONUS) utilizing high-resolution reanalysis, observational data, and numerical modeling to examine the influence of Q_P on precipitation and the surface energy budget. The findings indicate that the spatial distribution of Q_P climatology is analogous to that of precipitation, with magnitudes ranging from 2 to 3 W m^{-2} predominantly over the Midwest and Southeast regions. A seasonal analysis of Q_P reveals that the highest values occurring during the June–August (JJA) period, averaging 3.18 W m^{-2}. Peak Q_P values of approximately 4 W m^{-2} are observed during JJA over the Great Plains region. We hypothesize that the Q_P during an extreme precipitation event would be nonnegligible and have a significant impact on the local weather. To test this conjecture, we perform high-resolution simulations with and without Q_P during an extreme precipitation event over the Chicago Metropolitan Area (CMA). The results show that the Q_P may be a dominant factor compared to other components of surface heat flux during the zenith of precipitation hours. Also, Q_P has the potential to not only diminish precipitation but also alter and reconfigure the remaining surface energy budget components.

KEYWORDS: Precipitation; Energy budget/balance; Sensible heating; Urban meteorology

1. Introduction

As a vital component of the global hydrological cycle, precipitation has a worldwide impact with significant socioeconomic consequences (Zhou et al. 2011; McNeeley et al. 2012; Zhang et al. 2013; Stojanovic et al. 2021). Precipitation also affects salinity by introducing freshwater into the ocean, which accounts for most of the heat energy accumulation on Earth due to climate change by human activities (von Schuckmann et al. 2016). Over land, precipitation affects soil moisture, which in turn modulates the surface energy budget. Moreover, precipitation can play a crucial role in cooling the surface, as the temperature of raindrops is usually lower than that of the surface (Gosnell et al. 1995; Betts and Ball 1998; Kollet et al. 2009; Yin et al. 2014; Rooney et al. 2018; Liu et al. 2022). This surface sensible heat flux induced by precipitation (Q_P) remains an often-neglected feature in numerical models, and hence is typically excluded from the surface heat energy budget (Curry et al. 1999; Bittelli et al. 2008; Wei et al. 2014). The net surface heat flux is a crucial indicator of the intensity and spatial distribution of heat energy that can drive various natural processes in the land and ocean surfaces, lower atmosphere, and even biosphere (Anderson et al. 1998; Sengupta et al. 2002; Stephens et al. 2012; Valdivieso et al. 2017; Wild 2017, 2020; Zhou et al. 2020; Tomita et al. 2021; Zhou et al. 2022).

Heavier precipitation can result in significantly high Q_P, with implications for surface temperatures, surface heat energy budget, and local-to-regional scale circulations (Flament and Sawyer 1995; Gosnell et al. 1995; Anderson et al. 1998; Jacob and Koblinsky 2007; Kollet et al. 2009; Wei et al. 2014; Pinardi et al. 2016; Ramos et al. 2021). In low and midlatitudes, surface cooling due to heavy precipitation is often observed. For instance, Kollet et al. (2009) found that soil temperature decreased by more than 1 K after a heavy precipitation event in 2002 due to Q_P in a land surface model. Cong and Brady (2012) explored the negative correlations between heavy precipitation and surface temperature. According to Abera et al. (2020), anomalies in the surface temperature reliably and negatively responded to heavy precipitation events. The mean Q_P during the Tropical Ocean Global Atmosphere–Coupled Ocean–Atmosphere Response Experiment (TOGA-COARE) was found to be about 2.5 W m^{-2} (Gosnell et al. 1995). Ramos et al. (2021) showed that larger Q_P values (~2–3 W m^{-2}) are found over the intertropical convergence zone (ITCZ) and the South Pacific convergence zone (SPCZ). They also showed that during a typical Madden–Julian oscillation (MJO) event (Barrett et al. 2021) in April 2009 that produced precipitation exceeding 15 mm day^{-1} over the Maritime Continent (Tan et al. 2020, 2022a), Q_P was estimated to be >5 W m^{-2} over the coastal waters. Therefore, it is not a surprise that Q_P is not typically incorporated in state-of-art numerical weather and climate models. Nevertheless, Q_P can be substantial during heavy rainfall events. For instance, during TOGA-COARE, Q_P reached levels as high as 200 W m^{-2} for a

Denotes content that is immediately available upon publication as open access.

Corresponding author: Haochen Tan, htan@anl.gov

DOI: 10.1175/JHM-D-23-0068.1

precipitation event, which had a significant impact on the sea surface temperature (Gosnell et al. 1995). Anderson et al. (1998) also observed Q_P values ranging from 65 to 204 W m^{-2} during heavy rainfall events in the western Pacific warm pool in which Q_P played a notable role in modulating the net surface heat flux and surface buoyancy flux.

Outside the tropics, several studies (e.g., Boike et al. 2003; Gillett and Cullen 2011) have concluded that the Q_P has a crucial role in the process of glacier ablation and snow cover melt, by virtue of its ability to alter the albedo and thereby the absorption of solar radiation at the surface. These studies demonstrate that Q_P can have a significant impact on local near-surface temperature and surface energy budget. However, to the best of our knowledge, there are no prior studies with a comprehensive estimation of Q_P due to rainfall in the midlatitudes, especially over the contiguous United States (CONUS) on time scales of months or longer. One contributing factor to this knowledge gap regarding the estimation and influence of Q_P is the lack of observational data to compute Q_P. Additionally, current knowledge suggests that this influence from Q_P may be relatively minor. Hence, we first estimate the Q_P over CONUS using 20-yr reanalysis data to understand how Q_P can fully close the surface energy balance over the CONUS. We also examine the role of Q_P on other components of surface heat fluxes by using a regional climate model during an extreme precipitation event over the Chicago Metropolitan Area (CMA). The rest of the paper is organized as follows: methodology, data, and model are outlined in section 2. The results are in section 3, and the summary and conclusions are in section 4.

2. Methodology and data

a. Methods

The computation of sensible heat due to precipitation (Gosnell et al. 1995; Wei et al. 2014; Ramos et al. 2021) is based on the following:

$$Q_P = C_w \times \rho \times R \times (T_0 - T_r), \tag{1}$$

where C_w represents the specific heat of rainwater (4186 J kg^{-1} K^{-1}), ρ denotes the density of rainwater (1000 kg m^{-3}), R stands for the rain rate (m s^{-1}), T_0 refers the surface (land or ocean) temperature (°C), and T_r represents the temperature of raindrops (°C) when they reach the surface. The value of T_r can be estimated to be the wet bulb temperature (Byers et al. 1949; Kinzer and Gunn 1951; Katsaros and Buettner 1969; Kincaid and Longley 1989; Gosnell et al. 1995; Anderson et al. 1998; Wei et al. 2014). The wet bulb temperature can be obtained using the air temperature and relative humidity following Stull (2011):

$$\begin{aligned} T_r \cong T_w = {} & T \operatorname{atan}[0.151\,977 \times (\mathrm{RH}\% + 8.313\,659)^{0.5}] \\ & + \operatorname{atan}(T + \mathrm{RH}\%) - \operatorname{atan}(\mathrm{RH}\% - 1.676\,331) \\ & + 0.003\,918\,38 \times (\mathrm{RH}\%)^{1.5} \\ & \times \operatorname{atan}(0.023\,101 \times \mathrm{RH}\%) - 4.686\,035, \end{aligned} \tag{2}$$

where RH% is the relative humidity in percentage, T_w is the wet bulb temperature (°C), and T is the 2-m air temperature (°C).

The land surface energy balance is given by

$$\text{net heat flux} = \mathrm{Net_{SW}} - \mathrm{Net_{LW}} - \mathrm{LH} - \mathrm{SH} - G - Q_P, \tag{3}$$

where $\mathrm{Net_{LW}}$ is the net longwave radiation at the surface, $\mathrm{Net_{SW}}$ is the net shortwave radiation at the surface, LH is the latent heat flux, SH is the sensible heat flux, G is the ground heat flux, and Q_P is the sensible heat flux due to precipitation.

b. Observational and reanalysis data for estimating Q_P

Observed precipitation data are taken from National Centers for Environmental Prediction (NCEP) hourly 4-km gridded Stage IV quantitative precipitation estimates (QPEs; Nelson et al. 2016). The NCEP Stage IV QPEs contribute gridded multisensor precipitation estimates which combine Doppler radar estimates and observations from station gauges at a spatial resolution of about 4 km (Seo et al. 2010). Utilization of this high-resolution precipitation data will help us achieve a relatively accurate spatial variability of mean and extreme precipitation (Nelson et al. 2016; Beck et al. 2019). The relative humidity and air temperature are taken from NCEP North American Regional Reanalysis (NARR, 0.25° × 0.25°, monthly). For spatial and temporal consistency to the NARR dataset, the Stage IV data were averaged from 4 km to 0.25°, and from hourly to monthly. The calculations are performed for 2002–21.

3. Results

a. Climatological distribution

Figure 1 depicts the spatial variability of surface latent heat flux, sensible heat flux, net flux without Q_P, net heat flux with Q_P, mean precipitation, and Q_P over CONUS. The distribution of latent heat flux (Fig. 1a) reveals notable evaporation in the southeastern and eastern CONUS. The distribution of sensible heat flux (Fig. 1b) demonstrates a warmer environment over the southern CONUS, especially over the southern California, Arizona, New Mexico, and Texas. The incorporation of Q_P demonstrates that it helps better closing the surface energy budget, especially over the southeastern CONUS, which is also the area with higher precipitation than other regions (Figs. 1c–f). The precipitation over CONUS shows a west–east gradient from the Great Plains to the southeastern CONUS, with high precipitation also along the coastal mountain ranges in Northern California and the Sierra Nevada (Fig. 1e). The Q_P (Fig. 1f) shows a pattern similar to mean precipitation (Fig. 1e), with dominant precipitation confined to the Midwest and the Southeast regions, where the Q_P ranges from 2 to 3 W m^{-2}. This magnitude of Q_P is similar to that over the ITCZ, where long-term average of Q_P was found to be 2–3 W m^{-2} (Ramos et al. 2021). Higher Q_P values are also observed over Nebraska, Kansas, Oklahoma, and Texas, but the precipitation over these regions is not particularly high. This suggests that the relationship between Q_P

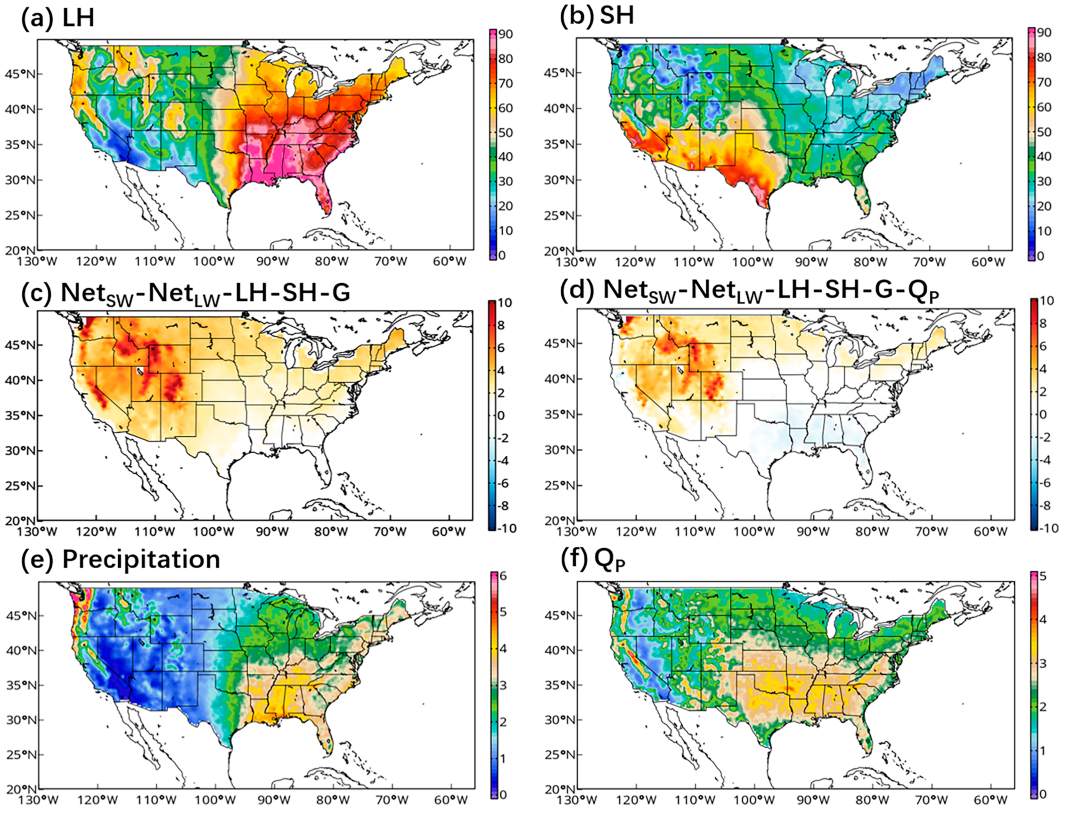

FIG. 1. (a) Averaged latent heat flux (LH; W m^{-2}), (b) sensible heat flux (SH; W m^{-2}), (c) net heat flux that does not incorporate with Q_P, (d) net heat flux incorporating Q_P, (e) precipitation (mm day^{-1}), and (f) sensible heat due to rain (Q_P; W m^{-2}) between 2002 and 2021 over CONUS. Surface flux components are from NARR data, precipitation is from NCEP Stage IV precipitation product, and Q_P is estimated from NARR and Stage IV precipitation data.

and precipitation may be nonlinear, which has also been reported in previous studies (Ramos et al. 2021). Climatologically, higher Q_P values are found in the central and eastern CONUS, where Q_P averages between 8% and 12% of the sensible heat flux (Fig. 2). However, the maximum Q_P over CONUS is dominant over the Great Plains region (Fig. 3), indicating that precipitation alone may not be the key factor influencing Q_P. Instead, the temperature difference between the surface and raindrop over this region may play a more significant role.

Figure 4 investigates the mean of precipitation and Q_P in six different regions chosen by the National Climate Assessment (NCA) (Fig. 4a). The result suggests that the variability of precipitation differs across the CONUS regions, with the Northwest (NW) and Southeast (SE) showing higher variability compared to other regions (Fig. 4b). The mean precipitation for each NCA region is estimated to be 3.0 mm day^{-1} for the Northeast, 2.66 mm day^{-1} for the Southeast, 2.55 mm day^{-1}

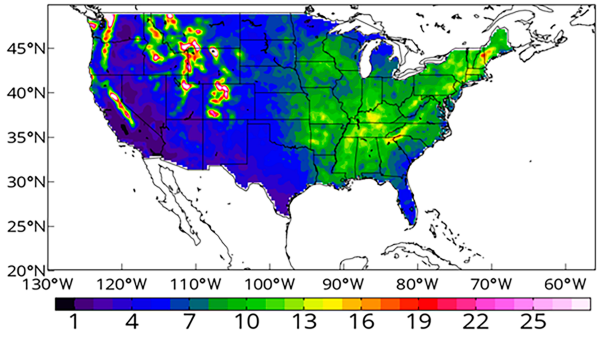

FIG. 2. Ratio between Q_P (W m^{-2}) and surface sensible heat flux (SH; W m^{-2}) during 2002–21. The unit is percentage.

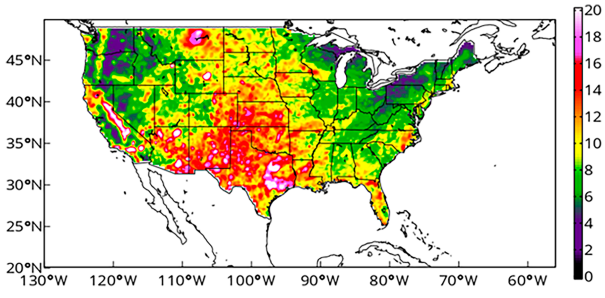

FIG. 3. Maximum Q_P (W m^{-2}) during 2002–21 over CONUS based on monthly data.

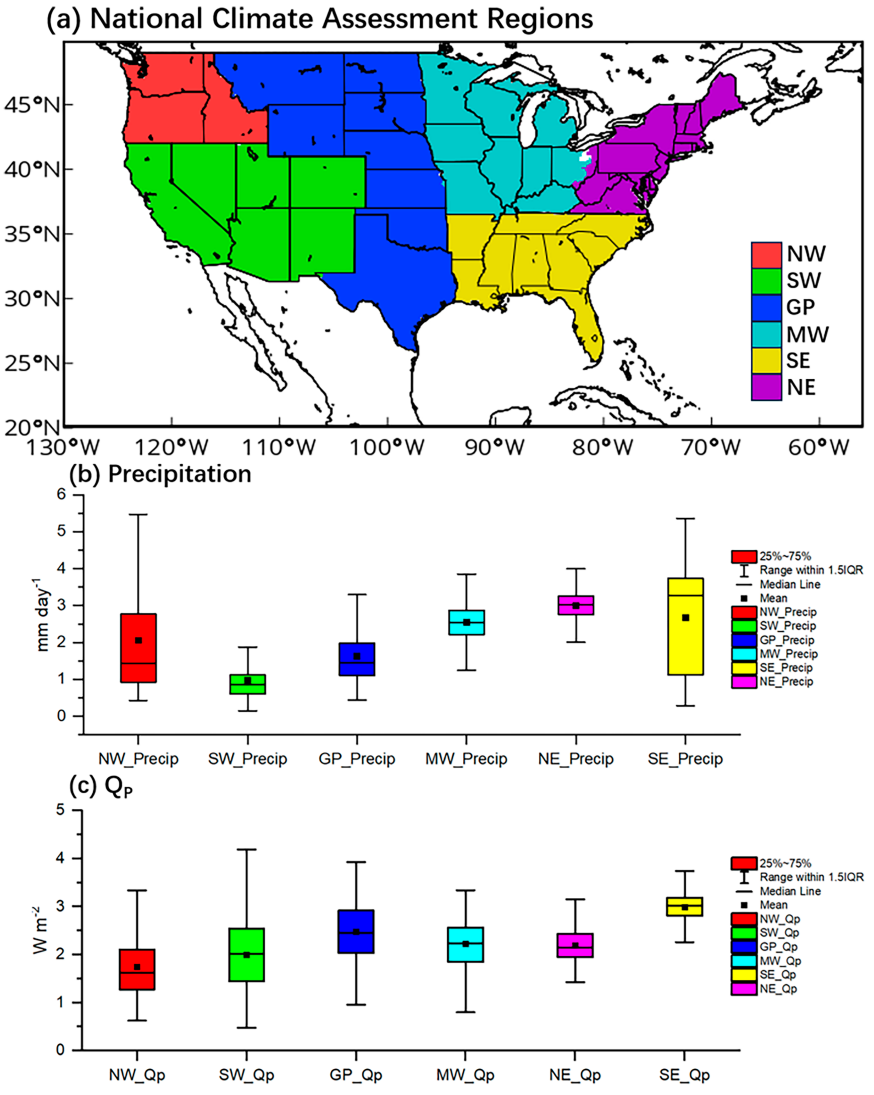

FIG. 4. (a) National Climate Assessment (NCA) regions. (b) Precipitation (mm day^{-1}) and (c) Q_P (W m^{-2}) for different NCA regions during 2002–21. The figure includes the interquartile range, the upper and lower extremes, the median, the mean, and the vertical lines outside the box extend to the 25th and 75th percentile.

for the Midwest, 2.0 mm day^{-1} for the Northwest, 1.62 mm day^{-1} for the Great Plains, and 0.97 mm day^{-1} for the Southwest. On the other hand, the Q_P varies in a different pattern, with the Southwest showing the highest variability, followed by Great Plains, Northwest, and Midwest (Fig. 4c). The results suggest that the higher precipitation does not necessarily translate into higher Q_P over land and is consistent with Ramos et al. (2021). To further understand the variability in Q_P, we discuss its seasonal cycle next.

b. Seasonal cycle

The mean Q_P (Fig. 5) for the seasons December–February (DJF), March–May (MAM), June–August (JJA), and September–November (SON) are 1.33, 2.55, 3.18, and 2.23 W m^{-2}, respectively. The maximum Q_P values of ~4 W m^{-2} are observed over the Great Plains region during JJA (Fig. 5c and Table 1). The magnitude of Q_P is also compared to SH in Table 1. From an annual perspective, the Q_P-to-SH ratio ranges between 5% and 10% across different regions, with the Northwest region exhibiting the smallest ratio and the Northeast region displaying the highest ratio. Among the seasons, DJF has the largest Q_P-to-SH ratio, particularly over the Southwest region where Q_P values can be as high as 41% of SH. The annual cycle of Q_P and SH over CONUS (Fig. 6) indicates that JJA has the highest Q_P values compared to other months. These results suggest Q_P may not be negligible and may help in closing the surface energy budget over the CONUS. This leads to a conjecture that Q_P may be significant during extreme precipitation events and may impact local weather. This conjecture is tested next over the CMA during an

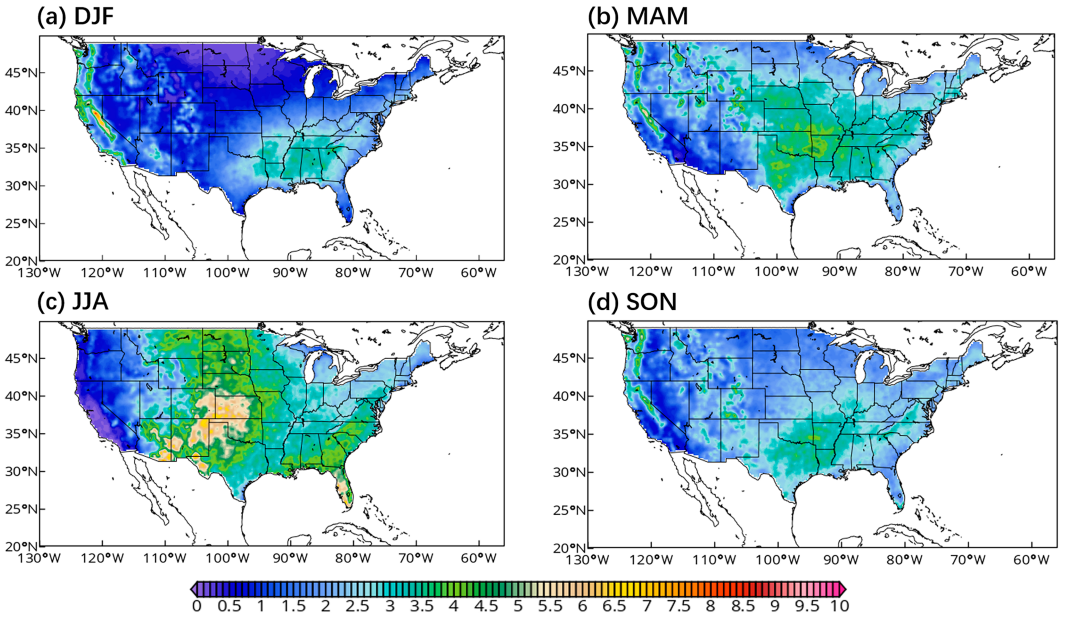

FIG. 5. Mean Q_P (W m^{-2}) over CONUS for (a) DJF, (b) MAM, (c) JJA, and (d) SON during 2002–21.

extreme rain event using high-resolution simulations with sophisticated urban parameterizations.

c. Q_P modulation

Moving forward from the comprehensive analysis of Q_P over the CONUS, it is pertinent to understand the implications of Q_P on a more granular level. While the previous analysis provided an overview of the spatial and temporal patterns at a continental scale, individual locales within the CONUS exhibit unique climatological characteristics that may respond differently to the influence of Q_P. Thus, it is imperative to delve into a case study that can illustrate the intricate role of Q_P on weather in a more localized scale.

Our site of choice for this purpose is the city of Chicago, Illinois, a location distinguished by its variable and sometimes extreme weather conditions, making it an ideal location for a more detailed examination. The transition from a broad study across the CONUS to an in-depth analysis of Chicago provides a useful pivot, allowing us to not only validate our findings but also explore the distinct microclimatic effects and their interactions with Q_P. We identified the Chicago Metropolitan Area as our primary study location for examining extreme rainfall events. This decision stems from multiple considerations: First, the region ranks among the most populated urban areas in the United States, thereby increasing its susceptibility to severe weather impacts. Furthermore, the significant influence of extreme weather on this region magnifies the implications of our research. We also chose to focus on urban settings due to their vulnerability to the destructive effects of intense precipitation, including infrastructural damage and loss of life. Additionally, urban areas, due to their heightened evaporation rates, can inadvertently contribute to augmented rainfall, a phenomenon known as urban-induced precipitation (Shepherd 2005, 2006; Mote et al. 2007; Shem and Shepherd 2009; Niyogi et al. 2011).

1) REGIONAL MODEL EXPERIMENTS

To explore the role of Q_P in modulating other surface energy budget terms and precipitation over the CMA during an extreme precipitation event, we used the nonhydrostatic and fully compressible Weather Research and Forecasting (WRF) Model (version 4.3.1; Skamarock et al. 2021) was utilized as the climate model for this study. To properly represent the

TABLE 1. Annual and seasonal means of Q_P, SH, and their ratio over CONUS from NARR and Stage IV data during 2002–21 (units in W m^{-2}).

	DJF			MAM			JJA			SON			Annual		
Regions	Q_P	SH	Q_P/SH	Q_P	SH	Q_P/SH	Q_P	SH	Q_P/SH	Q_P	SH	Q_P/SH	Q_P	SH	Q_P/SH
Northwest	1.4	8.1	17%	2.3	36.9	6%	1.3	69.9	2%	2.0	25.3	8%	1.7	35.0	5%
Southwest	1.4	3.5	40%	1.9	64.8	3%	2.7	93.3	3%	2.0	41.9	5%	2.0	50.8	4%
Great Plains	0.8	6.5	12%	2.8	53.7	5%	4.0	80.3	5%	2.3	34.5	7%	2.5	43.7	6%
Midwest	1.0	9.2	11%	2.7	35.5	8%	3.0	37.4	8%	2.2	25.7	8%	2.2	27.0	8%
Northeast	1.5	8.8	17%	2.5	33.0	8%	2.5	27.7	9%	2.2	20.0	11%	2.2	22.4	10%
Southeast	2.5	26.0	10%	3.0	41.1	7%	3.6	38.2	9%	2.7	33.1	8%	3.0	34.6	9%

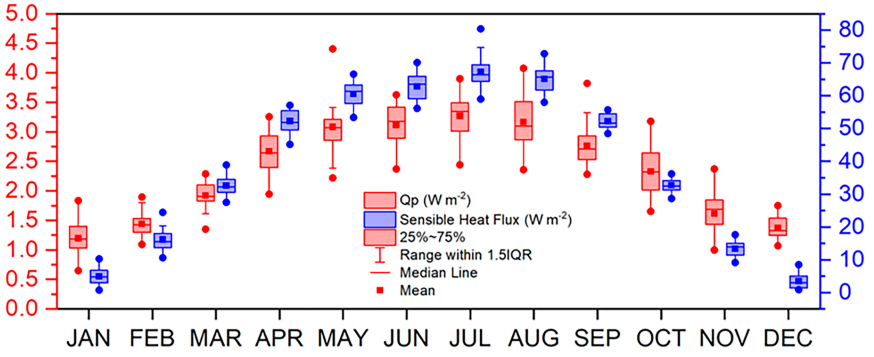

FIG. 6. Monthly averaged Q_P (W m^{-2}; red) and sensible heat flux (W m^{-2}; blue) over CONUS. Monthly averaging was based on 2002–21. The figure includes the interquartile range, the upper and lower extremes, the median, the mean, and the vertical lines outside the box extend to the 25th and 75th percentile.

CMA, the building effect parameterization coupled with the building energy model (BEP+BEM; Martilli et al. 2002) was employed. Thus, the deployment of BEP+BEM (Salamanca and Martilli 2010; Ribeiro et al. 2021; Segura et al. 2021; Tan et al. 2022b) is expected to provide a realistic surface energy budget over the urban area to better understand the effect of Q_P on other components of surface energy budget and local weather.

For simulations, three nested domains were used with varying number of horizontal grid points and spacing: 329 × 326 grid points in domain 1 with a spacing of 9 km, 634 × 571 in domain 2 with a spacing of 3 km, and 601 × 619 in domain 3 with a spacing of 1 km (Fig. 7a). The grid spacing of the outer domain (9 km) is expected to adequately capture synoptic-scale features inside the domain. The land-use data (Fig. 7b) was taken from the National Land Cover Database (Fig. 7b; Homer et al. 2015). The initial and boundary conditions were taken from the National Centers for Environmental Prediction Final Analysis data (NCEP-FNL, 1° × 1°, 6-hourly), and the unified Noah land surface model (Tewari et al. 2004) was used and modified by adding Q_P. The planetary boundary layer was modeled using the Mellor–Yamada–Janjić scheme outlined by Janjić (1994), while microphysics was simulated using the WRF single-moment 6-class microphysics scheme (Hong and Lim 2006). The shortwave radiation scheme employed was Dudhia's (1989) approach, whereas longwave radiation was modeled using the Rapid Radiative Transfer Model as presented by Mlawer et al. (1997). Additionally, the surface-layer scheme utilized the Monin–Obukhov–Janjić approach as described by Janjić (2002). Notably, no cumulus parameterization was employed in any simulations.

Two numerical experiments were conducted for a 2-day period during an extreme precipitation event from 1800 LST 12 September to 1800 LST 14 September 2008, to estimate the role of Q_P on other surface energy budget terms. The year 2008 stood out prominently as it not only holds the record for the highest annual precipitation in Chicago, but also marked a significant day on 13 September when the city

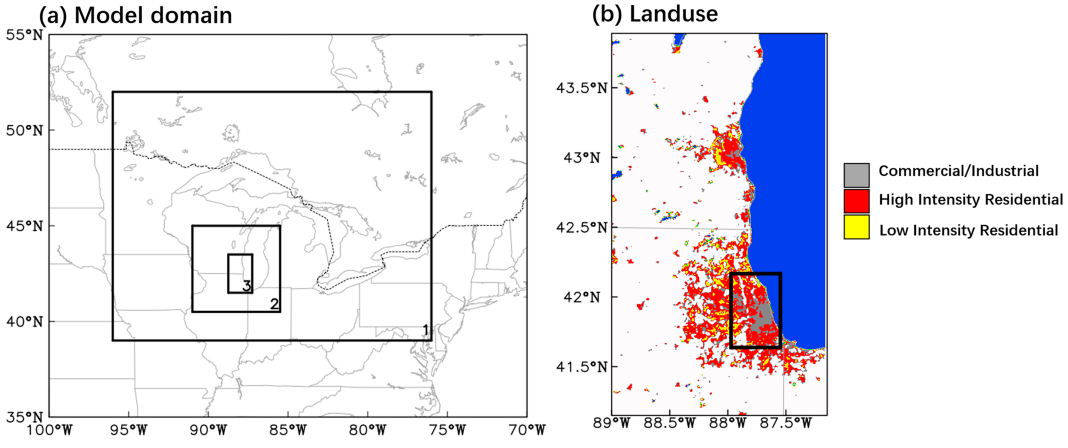

FIG. 7. (a) WRF domain configuration. The outer domain (1), the middle domain (2), and the inner domain (3) have horizontal grid spacings of 9, 3, and 1 km, respectively. (b) Urban land-use categories (shading) after the incorporation of the National Land Cover Database (NLCD) over domain 3. The black box in (b) is the CMA region. The blue color in (b) represents the water.

TABLE 2. Name and location of observational stations used in this study.

Station	Station name	Lat, lon (°N, °W)
1	KPDA West Chicago	41.881 83, 87.663 33
2	KMDW Chicago Midway Airport	41.784 17, 87.755 28
3	KORD Chicago O'Hare Airport	41.979 72, 87.904 44

registered a substantial rainfall of 6.64 in. Moreover, this daily rainfall figure is second only to one other occurrence in the period spanning from 2000 to 2023. The control (CTL) simulation was run without adding sensible heat due to precipitation into the model and the Qp_EXP was simulated after adding the sensible heat due to precipitation into the model.

2) EVALUATION OF CTL

The performance of CTL against data from multiple local stations concerning 2-m air temperature and 10-m horizontal wind, is exhibited in Tables 2 and 3. An analysis of the mean bias error (MBE) shows that CTL, when compared with three observational stations, indicates a deviation of 1.75°C, predominantly attributed to nighttime readings. This infers the model's propensity to yield a warm bias during the night. These biases represent systematic errors within the model, corroborated by several prior studies (Kim et al. 2013; Chen et al. 2014; Giovannini et al. 2014; Janicke et al. 2017; Wang et al. 2022; Tan et al. 2022b). In terms of wind speed, the primary source of low bias can be attributed to potential misclassifications that might arise between a model-derived grid cell and the physical footprint of the actual station.

The model's ability to capture the observed precipitation is shown in Fig. 8. Overall, the CTL reproduces precipitation distribution reasonably well except over the northeastern CMA where the model overestimates (Figs. 8a,b). The accumulated precipitation in model is also reasonable with a slight underestimation in the afternoon and an overestimation during early morning (Fig. 8c). Such temporal biases in capturing extreme precipitation are also documented by many other studies (Clark et al. 2007; Li et al. 2016; Tai et al. 2021; Gao et al. 2022; Tewari et al. 2022).

3) INFLUENCE OF Q_P ON PRECIPITATION AND SURFACE ENERGY BUDGET

Figure 9 depicts the hourly precipitation rate from observation, CTL, and Qp_EXP. The CTL has a delayed precipitation peak compared with observation from 1000 LST in OBS to 1200 LST in CTL. The precipitation is reduced in Qp_EXP compared to CTL in most times and this reduction is prominent during morning hours (~0200 LST) and noon (~1200 LST). This reduction in precipitation in Qp_EXP compared to CTL is due to Q_P-induced surface cooling that can lead to changes in atmospheric stability and moisture content, hence potentially affecting the formation and intensity of the precipitation.

Furthermore, Fig. 10 and Table 4 present the impact of Q_P inclusion in the model on surface energy budget terms. During the peak of precipitation (between 1000 and 1400 LST), Q_P reaches its maximum values (~14 W m^{-2}) at 1200 LST, dominating sensible and latent heat flux. In the CTL, the average sensible and latent heat flux values are 8.19 and 5.06 W m^{-2}, respectively (Table 4). However, after incorporating Q_P into the model, Qp_EXP produces an average Q_P value of 3.24 W m^{-2}, along with 10.79 W m^{-2} of sensible heat flux and 6.54 W m^{-2} of latent heat flux (Table 4) during the extreme precipitation event over CMA. Additionally, it is noteworthy that the sensible heat flux is also significantly modulated immediately after the peak of precipitation hours. For instance, in CTL, the sensible heat flux ranged from −30 to −5 W m^{-2} during 1300 to 1500 LST, while in Qp_EXP, it ranged from −15 to −8 W m^{-2}. The influence of Q_P on the sensible heat flux suggests its potential to significantly impact both latent and sensible heat flux. This is in line with the findings from a one-dimensional column experiment conducted by Kollet et al. (2009). However, in their study, the maximum differences for hourly fluxes reached up to 100 W m^{-2}. This occurred during and immediately after rainfall and evapotranspiration events.

TABLE 3. Mean bias error (MBE) and root-mean-square error (RMSE) of CTL against observational stations for 2-m temperature and 10-m winds during the day (0700–1900 LST), night (1900–0700 LST), and total on 13 Sep 2008.

Local stations	Time	2-m temperature (°C)		10-m wind (m s^{-1})	
		MBE	RMSE	MBE	RMSE
1, 2, 3	Total	1.75	2.44	−1.99	2.58
	Day	0.56	1.88	−1.23	2.01
	Night	1.19	2.62	−0.76	1.34

The inclusion of Q_P and its direct forcing led to surface cooling and less precipitation during this event, resulting in higher sensible and latent heat flux, but lower net longwave radiation and net shortwave radiation (Table 4). The stronger sensible heat flux may be attributed to stronger surface winds from enhanced local thermal circulations, as Q_P can generate a cooling effect. The weaker upward longwave radiation is due to the reduced surface temperature caused by Q_P. The Q_P has minimal impact on net shortwave radiation (Table 4). For a single heavy precipitation event, Q_P can significantly influence all components of surface fluxes for up to one month, and the cumulative influence of multiple events may be notable (Kollet et al. 2009). Our simulation was conducted for two days only. Therefore, how long the impact of Q_P from this extreme precipitation event would persist over the CMA is not known. We intend to investigate this aspect in the future.

4. Summary and discussion

This study examines the surface sensible heat flux resulting from precipitation (Q_P) by utilizing observational and reanalysis datasets over the CONUS. Furthermore, a mesoscale model is used to investigate the influence of Q_P on precipitation and surface energy budget. Analysis of the observational and reanalysis datasets reveals that Q_P has a similar spatial distribution as precipitation (Fig. 1), and its magnitude ranges from 2 to 3 W m^{-2} over the Midwest and Southeast regions.

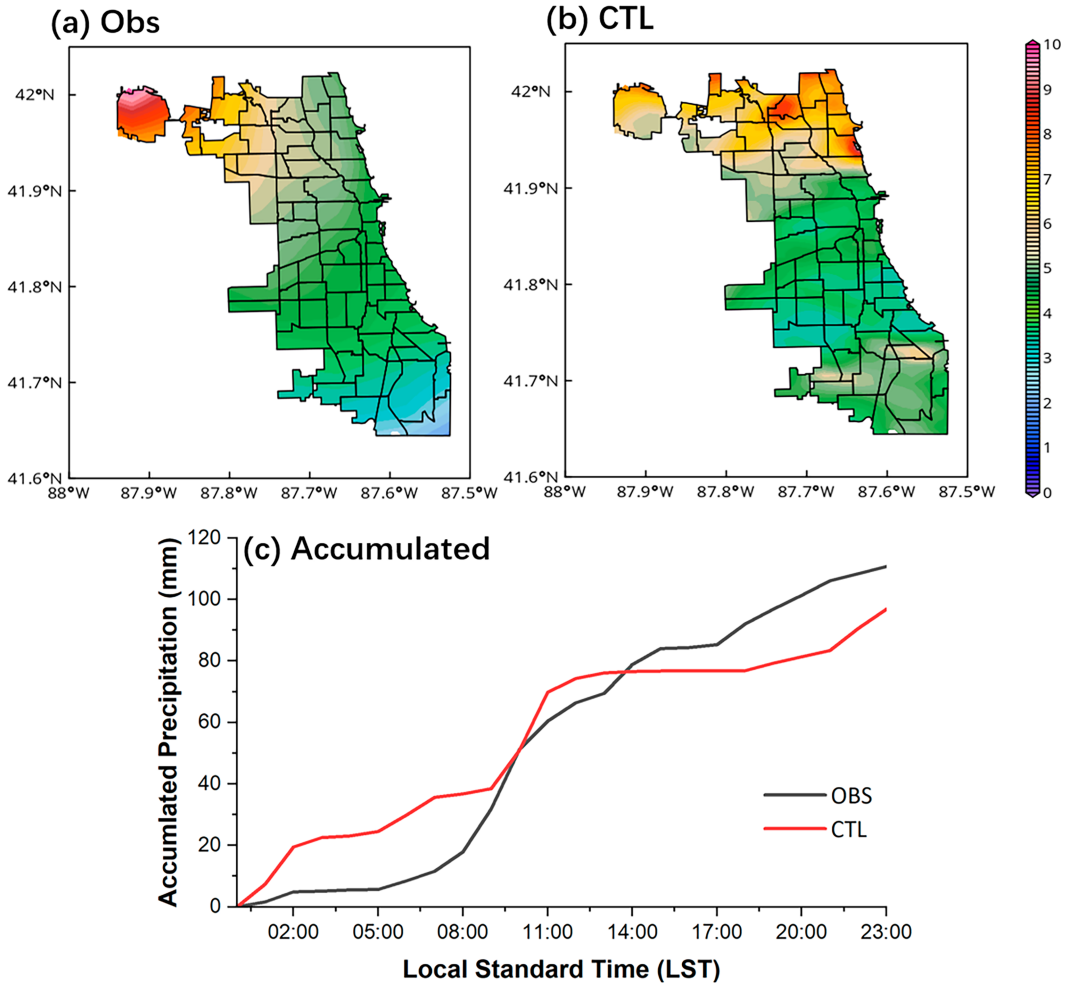

FIG. 8. Spatial distribution of rain rate (mm h^{-1}) over the CMA during 13 Sep 2008, from (a) observations and (b) CTL. (c) Accumulated precipitation (mm) calculated based on CMA only.

The greatest Q_P over the CONUS between 2002 and 2021 is observed predominantly over the Great Plains region, indicating that the temperature difference between surface and raindrop temperatures over this area may have a more substantial impact on Q_P than precipitation. Additionally, seasonal variation of Q_P demonstrates the highest values during JJA (3.18 W m^{-2}) over CONUS. The maximum Q_P is found to be ~4 W m^{-2} during JJA over the Great Plains region (Fig. 5c and Table 1). From an annual perspective, the Q_P-to-SH ratio ranges from 5% to

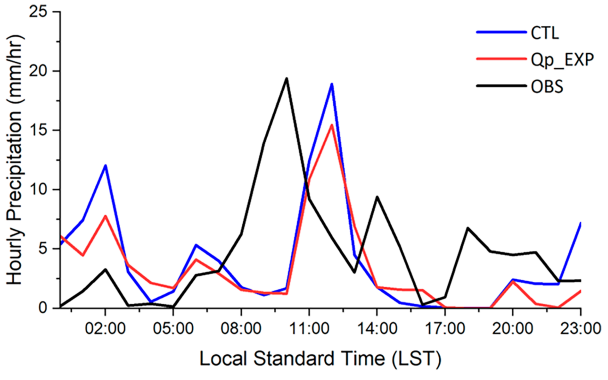

FIG. 9. Hourly precipitation (mm h^{-1}) for CTL (blue), Qp_EXP (red), and observation (black).

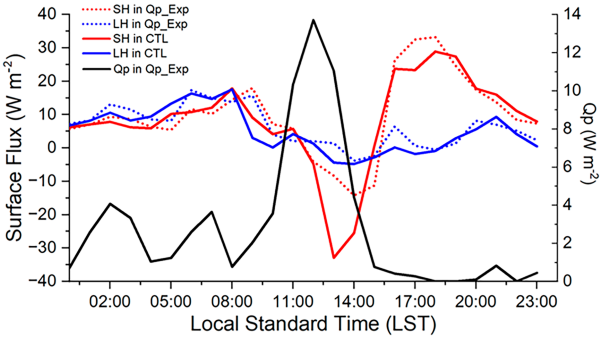

FIG. 10. Area-averaged latent heat (LH), sensible heat (SH), and Q_P (all in W m^{-2}) for 13 Sep 2008 over CMA.

TABLE 4. Surface heat flux components from the CTL and Qp_EXP over Chicago Metropolitan Area (CMA) during an extreme precipitation event on 13 Sep 2008.

Experiment	SH	LH	LW	SW	Q_P
CTL	8.19	5.06	5.88	40.91	—
Qp_EXP	10.79	6.54	4.99	39.74	3.24

10% across various regions, with the Northwest region displaying the lowest ratio and the Northeast region exhibiting the highest ratio (Table 1). Among the seasons, DJF has the highest Q_P-to-SH ratio, particularly over the Southwest region, where Q_P values can be as much as 40% of the SH. The annual cycle of Q_P and sensible heat flux indicates that JJA has higher Q_P values compared to other seasons. These results suggest Q_P may not be negligible and may help in closing the surface energy budget over the CONUS. This leads to a conjecture that Q_P may be significant during extreme precipitation events and may impact local weather. This conjecture is then tested over the CMA during an extreme rain event using high-resolution simulations with sophisticated urban parameterizations.

The modeling results show that Q_P can be the dominant term during the peak of precipitation hours. Q_P also modifies and redistribute the other surface energy budget terms. Such modulation is more pronounced for SH during the peak of precipitation hours, indicating that the Q_P can reduce the heat flow from the surface to the atmosphere. Moreover, inclusion of Q_P in the model leads to decline in simulated precipitation presumable due to increased stability due to cooler surface temperature. Using a global climate model, Wei et al. (2014) showed that the Q_P can also have some warming effects over midlatitude and high latitude in the northern winter by indirectly affecting land surface air temperature through changes in atmospheric circulations from weaker surface energy input gradient between equator and poles. From a surface energy budget perspective, incorporating Q_P can reduce the erroneous heating in all budget calculations, helping fully close the surface energy balance, and quantify the buoyancy forcing for both short and long-term periods. For example, Flament and Sawyer (1995) mentioned that 1 K yr^{-1} estimated erroneous heating in the mixed oceanic layer was produced by Q_P over tropical regions. Anderson et al. (1998) discovered that the 4-month averaged Q_P contributed to 15% of the net surface heat budget, leading to 6.5% less surface buoyancy. According to the findings of Kollet et al. (2009), the inclusion of Q_P in the analysis is crucial in achieving energy balance closure of observed fluxes. Hence, to achieve a closure of the surface energy balance and accurately quantify buoyancy forcing, it is imperative to incorporate the Q_P, despite its relatively minor contribution to the overall surface energy budget. Given the increasing occurrence of extreme precipitation events in the CONUS regions based on past data (Wu 2015; Fairman et al. 2016) and future projection data (Janssen et al. 2014, 2016; Prein et al. 2017; Zobel et al. 2018; Barlow et al. 2019; Lopez-Cantu et al. 2020), our study is expected to motivate future investigations on surface energy budget calculations from both observational and modeling perspectives.

Several important weaknesses of our Q_P simulations must be discussed. The first is related to the rainwater temperature used in Q_P computations. This value is not directly measured but approximated, utilizing wet bulb temperature within the simulations. This approximation introduces an element of uncertainty into the calculations, which could potentially be addressed by future technology capable of measuring rainwater temperature directly. A second limitation lies in the methodology, where the findings are based on a singular case simulation. A comprehensive climatological study considering diverse seasons would require considerable computational resources at a 1 km resolution, a scope that exceeds the limitations of the current study but will be contemplated for future research. Last, this study does not make use of more sophisticated urban land use data, specifically, the Local Climate Zones (LCZs). The LCZ is a level 0 product prepared by the World Urban Database and Access Portal Tools (WUDAPT; Ching et al. 2018), and it amalgamates various land use categories that have comparable long-term meteorological attributes. It provides a more nuanced classification of areas into 11 categories as opposed to the conventional three urban classifications. The incorporation of LCZs in a climatological run is planned.

While the influence of Q_P during short-time-scale extreme events is significant, the influence of Q_P on the long-term also cannot be ignored. The impact of Q_P is expected to be more pronounced in climate regimes characterized by numerous extreme convective precipitation events featuring substantial precipitation rates and significant temperature differences between the air and the land surface. To achieve a comprehensive understanding of Q_P, a more extensive climatological modeling study spanning several years is necessary. However, undertaking such a study with high resolution would necessitate a significant amount of computational time and is beyond the scope of the current investigation. Nonetheless, this remains an important avenue for future research.

Acknowledgments. This study is supported by COMPASS-GLM, a multi-institutional project supported by the U.S. Department of Energy (DOE), Office of Science, Office of Biological and Environmental Research as part of the Regional and Global Modeling and Analysis (RGMA) program, Multi-sector Dynamics Modeling (MSD) program, and Earth System Model Development (ESMD) program. We also acknowledge support from the CROCUS project funded by DOE BER under Contract DE-FOA-0002581. Computational resources are provided by the DOE-supported National Energy Research Scientific Computing Center and Argonne Leadership Computing Facility. PR acknowledges support from the Climate Program Office (CPO) of the National Oceanic and Atmospheric Administration (NOAA) through Grant NA22OAR4310612 and DOE through Grant DE-SC0023059. Computational resources are provided by the DOE-supported National Energy Research Scientific Computing Center and Argonne Leadership Computing Facility.

Data availability statement. The data that support the findings of this study are available from the following sources: 1) NCEP North American Regional Reanalysis (NARR): The NARR can be accessed through the https://psl.noaa.gov/data/gridded/data.narr.html. This dataset contains a high-resolution combined model and assimilated dataset from 1979 to near present at 8 times daily, daily, and monthly and is output on a Northern Hemisphere Lambert Conformal Conic grid. 2) NCEP/EMC 4 km Gridded Data Stage IV Data (ST4): The ST4 was obtained from https://data.eol.ucar.edu/dataset/21.093. The Stage IV analysis is based on the multisensor hourly/6-hourly 'Stage III' analyses (on local 4-km polar-stereographic grids) produced by the 12 River Forecast Centers (RFCs) in CONUS. NCEP mosaics the Stage III into a national product. Hourly, 6-hourly, and 24-hourly (accumulated from the 6-hourly) analyses are available. 3) Weather Research and Forecasting (WRF) Model: A detailed description the WRF Model can be found in http://doi.org/10.5065/1dfh-6p97. Please note that some restrictions apply to the availability of these datasets, as they were used under license or with permission from the respective data providers. Researchers interested in using these datasets are advised to contact the data providers to obtain appropriate permissions.

REFERENCES

Abera, T. A., J. Heiskanen, P. K. E. Pellikka, and E. E. Maeda, 2020: Impact of rainfall extremes on energy exchange and surface temperature anomalies across biomes in the Horn of Africa. *Agric. For. Meteor.*, **280**, 107779, https://doi.org/10.1016/j.agrformet.2019.107779.

Anderson, S. P., A. Hinton, and R. A. Weller, 1998: Moored observations of precipitation temperature. *J. Atmos. Oceanic Technol.*, **15**, 979–986, https://doi.org/10.1175/1520-0426(1998)015<0979:MOOPT>2.0.CO;2.

Barlow, M., and Coauthors, 2019: North American extreme precipitation events and related large-scale meteorological patterns: A review of statistical methods, dynamics, modeling, and trends. *Climate Dyn.*, **53**, 6835–6875, https://doi.org/10.1007/s00382-019-04958-z.

Barrett, B. S., C. R. Densmore, P. Ray, and E. R. Sanabia, 2021: Active and weakening MJO events in the maritime continent. *Climate Dyn.*, **57**, 157–172, https://doi.org/10.1007/s00382-021-05699-8.

Beck, H. E., and Coauthors, 2019: Daily evaluation of 26 precipitation datasets using Stage-IV gauge-radar data for CONUS. *Hydrol. Earth Syst. Sci.*, **23**, 207–224, https://doi.org/10.5194/hess-23-207-2019.

Betts, A. K., and J. H. Ball, 1998: FIFE surface climate and site-average dataset 1987–89. *J. Atmos. Sci.*, **55**, 1091–1108, https://doi.org/10.1175/1520-0469(1998)055<1091:FSCASA>2.0.CO;2.

Bittelli, M., F. Ventura, G. S. Campbell, R. L. Snyder, F. Gallegati, and P. R. Pisa, 2008: Coupling of heat, water vapor, and liquid water fluxes to compute evaporation in bare soils. *J. Hydrol.*, **362**, 191–205, https://doi.org/10.1016/j.jhydrol.2008.08.014.

Boike, J., K. Roth, and O. Ippisch, 2003: Seasonal snow cover on frozen ground: Energy balance calculations of a permafrost site near Ny-Ålesund, Spitsbergen. *J. Geophys. Res.*, **108**, 8163, https://doi.org/10.1029/2001JD000939.

Byers, H. R., H. Moses, and P. J. Harney, 1949: Measurement of air temperature. *J. Meteor.*, **6**, 51–55, https://doi.org/10.1175/1520-0469(1949)006<0051:MORT>2.0.CO;2.

Chen, F., X. Yang, and W. Zhu, 2014: WRF simulations of urban heat island under hot-weather synoptic conditions: The case study of Hangzhou City, China. *Atmos. Res.*, **138**, 364–377, https://doi.org/j.atmosres.2013.12.005.

Ching, J., and Coauthors, 2018: WUDAPT: An urban weather, climate, and environmental modeling infrastructure for the Anthropocene. *Bull. Amer. Meteor. Soc.*, **99**, 1907–1924, https://doi.org/10.1175/BAMS-D-16-0236.1.

Clark, A. J., W. A. Gallus Jr., and T.-C. Chen, 2007: Comparison of the diurnal precipitation cycle in convection-resolving and non-convection-resolving mesoscale models. *Mon. Wea. Rev.*, **135**, 3456–3473, https://doi.org/10.1175/MWR3467.1.

Cong, R.-G., and M. Brady, 2012: The interdependence between rainfall and temperature: Copula analyses. *Sci. World J.*, **2012**, 405675, https://doi.org/10.1100/2012/405675.

Curry, J. A., C. A. Clayson, W. B. Rossow, R. Reeder, Y. Zhang, P. J. Webster, G. Liu, and R. Sheu, 1999: High-resolution satellite-derived dataset of the surface fluxes of heat, freshwater, and momentum for the TOGA COARE IOP. *Bull. Amer. Meteor. Soc.*, **80**, 2059–2080, https://doi.org/10.1175/1520-0477(1999)080<2059:HRSDDO>2.0.CO;2.

Dudhia, J., 1989: Numerical study of convection observed during the Winter Monsoon Experiment using a mesoscale two-dimensional model. *J. Atmos. Sci.*, **46**, 3077–3107, https://doi.org/10.1175/1520-0469(1989)046<3077:NSOCOD>2.0.CO;2.

Fairman, J. G., Jr., D. M. Schultz, D. J. Kirshbaum, S. L. Gray, and A. I. Barrett, 2016: Climatology of banded precipitation over the contiguous United States. *Mon. Wea. Rev.*, **144**, 4553–4568, https://doi.org/10.1175/MWR-D-16-0015.1.

Flament, P., and M. Sawyer, 1995: Observations of the effect of rain temperature on the surface heat flux in the intertropical convergence zone. *J. Phys. Oceanogr.*, **25**, 413–419, https://doi.org/10.1175/1520-0485(1995)025<0413:OOTEOR>2.0.CO;2.

Gao, L., J. Wei, X. Lei, M. Ma, L. Wang, X. Guan, and H. Lin, 2022: Simulation of an extreme precipitation event using ensemble-based WRF model in the southeastern coastal region of China. *Atmosphere*, **13**, 194, https://doi.org/10.3390/atmos13020194.

Gillett, S., and N. J. Cullen, 2011: Atmospheric controls on summer ablation over Brewster Glacier, New Zealand. *Int. J. Climatol.*, **31**, 2033–2048, https://doi.org/10.1002/joc.2216.

Giovannini, L., D. Zardi, M. de Franceschi, and F. Chen, 2014: Numerical simulations of boundary-layer processes and urban-induced alterations in an Alpine valley. *Int. J. Climatol.*, **34**, 1111–1131, https://doi.org/10.1002/joc.3750.

Gosnell, R., C. W. Fairall, and P. J. Webster, 1995: The sensible heat of rainfall in the tropical ocean. *J. Geophys. Res.*, **100**, 18 437–18 442, https://doi.org/10.1029/95JC01833.

Homer, C. G., and Coauthors, 2015: Completion of the 2011 National Land Cover Database for the conterminous United States—Representing a decade of land cover change information. *Photogramm. Eng. Remote Sens.*, **81**, 345–354, https://doi.org/10.1016/S0099-1112(15)30100-2.

Hong, S.-Y., and J.-O. J. Lim, 2006: The WRF single-moment 6-class microphysics scheme (WSM6). *J. Korean Meteor. Soc.*, **42**, 129–151.

Jacob, S. D., and C. J. Koblinsky, 2007: Effects of precipitation on the upper-ocean response to a hurricane. *Mon. Wea. Rev.*, **135**, 2207–2225, https://doi.org/10.1175/MWR3366.1.

Janicke, B., F. Meier, D. Fenner, U. Fehrenbach, A. Holtmann, and D. Scherer, 2017: Urban–rural differences in near-surface air temperature as resolved by the Central Europe Refined analysis (CER): Sensitivity to planetary boundary layer schemes and urban canopy models. *Int. J. Climatol.*, **37**, 2063–2079, https://doi.org/10.1002/joc.4835.

Janjić, Z. I., 1994: The Step-Mountain Eta Coordinate Model: Further developments of the convection, viscous sublayer, and turbulence closure schemes. *Mon. Wea. Rev.*, **122**, 927–945, https://doi.org/10.1175/1520-0493(1994)122<0927:TSMECM>2.0.CO;2.

——, 2002: Nonsingular implementation of the Mellor–Yamada level 2.5 scheme in the NCEP Meso model. NCEP Office Note 437, 61 pp., http://www.emc.ncep.noaa.gov/officenotes/newernotes/on437.pdf.

Janssen, E., D. J. Wuebbles, K. E. Kunkel, S. C. Olsen, and A. Goodman, 2014: Observational- and model-based trends and projections of extreme precipitation over the contiguous United States. *Earth's Future*, **2**, 99–113, https://doi.org/10.1002/2013EF000185.

——, R. L. Sriver, D. J. Wuebbles, and K. E. Kunkel, 2016: Seasonal and regional variations in extreme precipitation event frequency using CMIP5. *Geophys. Res. Lett.*, **43**, 5385–5393, https://doi.org/10.1002/2016GL069151.

Katsaros, K., and J. K. Buettner, 1969: Influence of rainfall on temperature and salinity of the ocean surface. *J. Appl. Meteor.*, **8**, 15–18, https://doi.org/10.1175/1520-0450(1969)008<0015:IOROTA>2.0.CO;2.

Kim, Y., K. Sartelet, J. C. Raut, and P. Chazette, 2013: Evaluation of the weather research and forecast/urban model over greater Paris. *Boundary-Layer Meteor.*, **149**, 105–132, https://doi.org/10.1007/s10546-013-9838-6.

Kincaid, D. C., and T. S. Longley, 1989: A water droplet evaporation and temperature model. *Trans. ASAE*, **32**, 457–463, https://doi.org/10.13031/2013.31026.

Kinzer, G. D., and R. Gunn, 1951: The evaporation, temperature, and thermal relaxation-time of freely falling water drops. *J. Atmos. Sci.*, **8**, 71–83, https://doi.org/10.1175/1520-0469(1951)008<0071:TETATR>2.0.CO;2.

Kollet, S. J., I. Cvijanovic, D. Schuettemeyer, R. M. Maxwell, A. F. Moene, and P. Bayer, 2009: The influence of rain sensible heat and subsurface energy transport on the energy balance at the land surface. *Vadose Zone J.*, **8**, 846–857, https://doi.org/10.2136/vzj2009.0005.

Li, Y., G. Lu, Z. Wu, H. He, J. Shi, J. Shi, Y. Ma, and S. Weng, 2016: Evaluation of optimized WRF precipitation forecast over a complex topography region during flood season. *Atmosphere*, **7**, 145, https://doi.org/10.3390/atmos7110145.

Liu, W., S. Dong, J. Zheng, C. Liu, C. Wang, S. Wei, Y. Zhang, and Y. Zhang, 2022: Quantifying the rainfall cooling effect: The importance of relative humidity in Guangdong, South China. *J. Hydrometeor.*, **23**, 875–889, https://doi.org/10.1175/JHM-D-21-0155.1.

Lopez-Cantu, T., A. F. Prein, and C. Samaras, 2020: Uncertainties in future U.S. extreme precipitation from downscaled climate projections. *Geophys. Res. Lett.*, **47**, e2019GL086797, https://doi.org/10.1029/2019GL086797.

Martilli, A., A. Clappier, and M. W. Rotach, 2002: An urban surface exchange parameterisation for mesoscale models. *Bound.-Layer Meteor.*, **104**, 261–304, https://doi.org/10.1023/A:1016099921195.

McNeeley, S. M., and Coauthors, 2012: Catalyzing frontiers in water-climate-society research: A view from early career scientists and junior faculty. *Bull. Amer. Meteor. Soc.*, **93**, 477–484, https://doi.org/10.1175/BAMS-D-11-00221.1.

Mlawer, E. J., S. J. Taubman, P. D. Brown, M. J. Iacono, and S. A. Clough, 1997: Radiative transfer for inhomogeneous atmospheres: RRTM, a validated correlated-k model for the longwave. *J. Geophys. Res.*, **102**, 16 663–16 682, https://doi.org/10.1029/97JD00237.

Mote, T. L., C. L. Matthew, and J. M. Shepherd, 2007: Radar signatures of the urban effect on precipitation distribution: A case study for Atlanta, Georgia. *Geophys. Res. Lett.*, **34**, L20710, https://doi.org/10.1029/2007GL031903.

Nelson, B. R., O. P. Prat, D.-J. Seo, and E. Habib, 2016: Assessment and implications of NCEP Stage IV quantitative precipitation estimates for product intercomparisons. *Wea. Forecasting*, **31**, 371–394, https://doi.org/10.1175/WAF-D-14-00112.1.

Niyogi, D., P. Pyle, M. Lei, S. P. Arya, C. M. Kishtawal, M. Shepherd, F. Chen, and B. Wolfe, 2011: Urban modification of thunderstorms: An observational storm climatological and model case study for the Indianapolis urban region. *J. Appl. Meteor. Climatol.*, **50**, 1129–1144, https://doi.org/10.1175/2010JAMC1836.1.

Pinardi, N., and Coauthors, 2016: Marine rapid environmental assessment in the Gulf of Taranto: A multiscale approach. *Nat. Hazards Earth Syst. Sci.*, **16**, 2623–2639, https://doi.org/10.5194/nhess-16-2623-2016.

Prein, A., R. M. Rasmussen, K. Ikeda, C. Liu, M. P. Clark, and G. J. Holland, 2017: The future intensification of hourly precipitation extremes. *Nat. Climate Change*, **7**, 48–52, https://doi.org/10.1038/nclimate3168.

Ramos, C. G. M., H. Tan, P. Ray, and J. Dudhia, 2021: Estimates of the sensible heat of rainfall in the tropics from reanalysis and observations. *Int. J. Climatol.*, **42**, 2246–2259, https://doi.org/10.1002/joc.7363.

Ribeiro, I., A. Martilli, M. Falls, A. Zonato, and G. Villaba, 2021: Highly resolved WRF-BEP/BEM simulations over Barcelona urban area with LCZ. *Atmos. Res.*, **248**, 105220, https://doi.org/10.1016/j.atmosres.2020.105220.

Rooney, G. G., N. van Lipzig, and W. Thiery, 2018: Estimating the effect of rainfall on the surface temperature of a tropical lake. *Hydrol. Earth Syst. Sci.*, **22**, 6357–6369, https://doi.org/10.5194/hess-22-6357-2018.

Salamanca, F., and A. Martilli, 2010: A new building energy model coupled with an urban canopy parameterization for urban climate simulations—Part II. Validation with one-dimensional off-line simulations. *Theor. Appl. Climatol.*, **99**, 345–356, https://doi.org/10.1007/s00704-009-0143-8.

Segura, R., A. Badia, S. Ventura, J. Gilabert, A. Martilli, and G. Villalba, 2021: Sensitivity study of PBL schemes and soil initialization using the WRF-BEP-BEM model over a Mediterranean coastal city. *Urban Climate*, **39**, 100982, https://doi.org/10.1016/j.uclim.2021.100982.

Sengupta, D., P. Ray, and G. S. Bhat, 2002: Spring warming of the eastern Arabian Sea and Bay of Bengal from buoy data. *Geophys. Res. Lett.*, **29**, 1734, https://doi.org/10.1029/2002GL015340.

Seo, D.-J., A. Seed, and G. Delrieu, 2010: Radar and multisensor rainfall estimation for hydrologic applications. *Rainfall: State of the Science*, *Geophys. Monogr.*, Vol. 191, Amer. Geophys. Union, 79–104, https://doi.org/10.1029/2010GM000952.

Shem, W., and M. Shepherd, 2009: On the impact of urbanization on summertime thunderstorms in Atlanta: Two numerical model case studies. *Atmos. Res.*, **92**, 172–189, https://doi.org/10.1016/j.atmosres.2008.09.013.

Shepherd, J. M., 2005: A review of current investigations of urban-induced rainfall and recommendations for the future. *Earth Interact.*, **9**, https://doi.org/10.1175/EI156.1.

——, 2006: Evidence of urban-induced precipitation variability in arid climate regimes. *J. Arid Environ.*, **67**, 607–628, https://doi.org/10.1016/j.jaridenv.2006.03.022.

Skamarock, W. C., and Coauthors, 2021: A description of the Advanced Research WRF Model version 4.3. NCAR Tech. Note NCAR/TN-556+STR, 145 pp., https://doi.org/10.5065/1dfh-6p97.

Stephens, G. L., and Coauthors, 2012: An update on Earth's energy balance in light of the latest global observations. *Nat. Geosci.*, **5**, 691–696, https://doi.org/10.1038/ngeo1580.

Stojanovic, M., A. Gonçalves, R. Sorí, M. Vázquez, A. M. Ramos, R. Nieto, L. Gimeno, and M. L. R. Liberato, 2021: Consecutive extratropical cyclones Daniel, Elsa and Fabien, and their impact on the hydrological cycle of mainland Portugal. *Water*, **13**, 1476, https://doi.org/10.3390/w13111476.

Stull, R., 2011: Wet-bulb temperature from relative humidity and air temperature. *J. Appl. Meteor. Climatol.*, **50**, 2267–2269, https://doi.org/10.1175/JAMC-D-11-0143.1.

Tai, S.-L., Z. Feng, P.-L. Ma, C. Schumacher, and J. D. Fast, 2021: Representations of precipitation diurnal cycle in the Amazon as simulated by observationally constrained cloud-system resolving and global climate models. *J. Adv. Model. Earth Syst.*, **13**, e2021MS002586, https://doi.org/10.1029/2021MS002586.

Tan, H., P. Ray, B. S. Barrett, M. Tewari, and M. W. Moncrieff, 2020: Role of topography on the MJO in the maritime continent: a numerical case study. *Climate Dyn.*, **55**, 295–314, https://doi.org/10.1007/s00382-018-4275-3.

——, ——, B. Barrett, J. Dudhia, M. Moncrieff, L. Zhang, and D. Zermeno-Diaz, 2022a: Understanding the role of topography on the diurnal cycle of precipitation in the Maritime Continent during MJO propagation. *Climate Dyn.*, **58**, 3003–3019, https://doi.org/10.1007/s00382-021-06085-0.

——, V. R. Kotamarthi, J. Wang, Y. Qian, and T. C. Chakraborty, 2022b: Impact of different roofing mitigation strategies on near-surface temperature and energy consumption over the Chicago metropolitan area during a heatwave event. *Sci. Total Environ.*, **860**, 160508, https://doi.org/10.1016/j.scitotenv.2022.160508.

Tewari, M., and Coauthors, 2004: Implementation and verification of the unified NOAH land surface model in the WRF model. *20th Conf. on Weather Analysis and Forecasting/16th Conf. on Numerical Weather Prediction*, Seattle, WA, Amer. Meteor. Soc., 14.2a, https://ams.confex.com/ams/84Annual/techprogram/paper_69061.htm.

——, F. Chen, J. Dudhia, P. Ray, S. Miao, E. Nikolopoulos, and L. Treinish, 2022: Understanding the sensitivity of WRF hindcast of Beijing extreme rainfall of 21 July 2012 to microphysics and model initial time. *Atmos. Res.*, **271**, 106085, https://doi.org/10.1016/j.atmosres.2022.106085.

Tomita, H., K. Kutsuwada, M. Kubota, and T. Hihara, 2021: Advances in the estimation of global surface net heat flux based on satellite observation: J-OFURO3 V1.1. *Front. Mar. Sci.*, **8**, 612361, https://doi.org/10.3389/fmars.2021.612361.

Valdivieso, M., and Coauthors, 2017: An assessment of air–sea heat fluxes from ocean and coupled reanalyses. *Climate Dyn.*, **49**, 983–1008, https://doi.org/10.1007/s00382-015-2843-3.

von Schuckmann, K., and Coauthors, 2016: An imperative to monitor Earth's energy imbalance. *Nat. Climate Change*, **6**, 138–144, https://doi.org/10.1038/nclimate2876.

Wang, X., H. Li, and S. Sodoudi, 2022: The effectiveness of cool and green roofs in mitigating urban heat island and improving human thermal comfort. *Build. Environ.*, **217**, 109082, https://doi.org/10.1016/j.buildenv.2022.109082.

Wei, N., Y. Dai, M. Zhang, L. Zhou, D. Ji, S. Zhu, and L. Wang, 2014: Impact of precipitation-induced sensible heat on the simulation of land-surface air temperature. *J. Adv. Model. Earth Syst.*, **6**, 1311–1320, https://doi.org/10.1002/2014MS000322.

Wild, M., 2017: Towards global estimates of the surface energy budget. *Curr. Climate Change Rep.*, **3**, 87–97, https://doi.org/10.1007/s40641-017-0058-x.

——, 2020: The global energy balance as represented in CMIP6 climate models. *Climate Dyn.*, **55**, 553–577, https://doi.org/10.1007/s00382-020-05282-7.

Wu, S.-Y., 2015: Changing characteristics of precipitation for the contiguous United States. *Climatic Change*, **132**, 677–692, https://doi.org/10.1007/s10584-015-1453-8.

Yin, D., M. L. Roderick, G. Leech, F. Sun, and Y. Huang, 2014: The contribution of reduction in evaporative cooling to higher surface air temperatures during drought. *Geophys. Res. Lett.*, **41**, 7891–7897, https://doi.org/10.1002/2014GL062039.

Zhang, Q., J. Li, V. P. Singh, and M. Xiao, 2013: Spatio-temporal relations between temperature and precipitation regimes: Implications for temperature-induced changes in the hydrological cycle. *Global Planet. Change*, **111**, 57–76, https://doi.org/10.1016/j.gloplacha.2013.08.012.

Zhou, X., P. Ray, B. S. Barrett, and P.-C. Hsu, 2020: Understanding the bias in surface latent and sensible heat fluxes in contemporary AGCMs over tropical oceans. *Climate Dyn.*, **55**, 2957–2978, https://doi.org/10.1007/s00382-020-05431-y.

——, ——, B. Barrett, and P.-C. Hsu, 2022: Systematic improvement in simulated surface latent and sensible heat fluxes over tropical oceans in AMIP6 models compared to AMIP5 models with the same resolutions. *Atmos. Res.*, **274**, 106214, https://doi.org/10.1016/j.atmosres.2022.106214.

Zhou, Y. P., K.-M. Xu, Y. C. Sud, and A. K. Betts, 2011: Recent trends of the tropical hydrological cycle inferred from Global Precipitation Climatology Project and International Satellite Cloud Climatology Project data. *J. Geophys. Res.*, **116**, D09101, https://doi.org/10.1029/2010JD015197.

Zobel, Z., J. Wang, D. J. Wuebbles, and V. R. Kotamarthi, 2018: Analyses for high-resolution projections through the end of the 21st century for precipitation extremes over the United States. *Earth's Future*, **6**, 1471–1490, https://doi.org/10.1029/2018EF000956.